

Electrostatic Self-assembly of MXene and Carbon Nanotube@MnO₂ Multilevel Hybrids for Achieving Fast Charge Storage Kinetics in Aqueous Asymmetric Supercapacitors

Shulong Li¹, Zhongyou Peng¹, Yuting Huang¹, Licheng Tan^{1,*}, Yiwang Chen^{1,2*}

S. Li, Z. Peng, Y. Huang, Prof. Dr. L. Tan, Prof. Dr. Y. Chen

¹ College of Chemistry and Chemical Engineering/Institute of Polymers and Energy Chemistry (IPEC), Nanchang University, 999 Xuefu Avenue, Nanchang 330031, China.

² National Engineering Research Center for Carbohydrate Synthesis/Key Lab of Fluorine and Silicon for Energy Materials and Chemistry of Ministry of Education, Jiangxi Normal University, 99 Ziyang Avenue, Nanchang 330022, China.

*Corresponding Authors: tanlicheng@ncu.edu.cn (L. Tan); ywchen@ncu.edu.cn (Y. Chen).

Calculations

The gravimetric capacitance (C_g) is calculated by the following equation:

$$C_g = \frac{1}{\Delta V m v} \int i dV = \frac{I \Delta t}{\Delta V} \quad (1)$$

where i is the response current density, V is the potential window, v is the potential scan rate, and m is the mass of the active material, I is the current density, Δt is the discharge time. According to the following equation to calculate the gravimetric energy density (E_g) and power density (P_g)

$$E_g = \frac{0.5 C V^2}{3.6} \quad (2)$$

$$P_g = \frac{3600 E}{\Delta t} \quad (3)$$

The volumetric capacity (C_V) was obtained from the following equation

$$C_V = \rho C_g \quad (4)$$

where ρ is the density of the films, which was calculated assuming:

$$\rho = \frac{m}{Sd} \quad (5)$$

where m , S and d are the mass, area and thickness of the electrode, respectively.

The volumetric energy (E_V), and power densities (P_V), were calculated assuming:

$$E_V = \rho E_g \quad (6)$$

$$P_V = \rho P_g \quad (7)$$

Generally, the relationship between i_p and v follows the power law:

$$i_p = a v^b \quad (8)$$

a , b , k_1 and k_2 are configurable parameters. If $b = 0.5$, the energy storage is implied to be completely controlled by diffusive behavior. And if $b = 1$, the energy storage is implied to be completely controlled by non-diffusive behavior. The contributions of the two mechanisms at different scanning rates are further quantified by calculating the k_1 and k_2 values according to the following equation:

$$i_p = k_1 + k_2 v^{0.5} \quad (9)$$

The total stored charge (q_T) consists of outer surface charges and inner surface charges. The charge

storage on the outer surface is independent of the sweep rate and non-diffusion-controlled, while the charge storage on the inner surface is a diffusion-controlled process. Therefore, the total measured charge can be presented into a function of the sweep rate (v) by the following equations:

$$q_T = q_o + q_i \quad (10)$$

$$q_T = q_\infty + kv^{-1/2} \quad (11)$$

The real $C'(\omega)$ and imaginary part $C''(\omega)$ capacitances can be calculated through the following equations

$$C'(\omega) = \frac{-Z''(\omega)}{\omega|Z(\omega)|^2} \quad (12)$$

$$C''(\omega) = \frac{Z'(\omega)}{\omega|Z(\omega)|^2} \quad (13)$$

where $Z'(\omega)$, $Z''(\omega)$ and ω are the respective real and imaginary parts of the complex impedance $Z(\omega)$ and angular frequency given by $\omega = 2\pi f$.

The experimental ion population change ($\Delta\Gamma_{exp}$) was calculated by the following equation:

$$\Delta\Gamma_{exp} = \frac{\Delta m}{M_i} \quad (14)$$

The change in the theoretical ion population can be calculated by Faraday's law as follow:

$$\Delta\Gamma_{theor} = \frac{\Delta Q}{nF} \quad (15)$$

where ΔQ is the charge passed through the electrode (C), M is the molar weight of the ions, F is the Faraday constant (96485 C mol^{-1}), and n is the valence number of the ion.

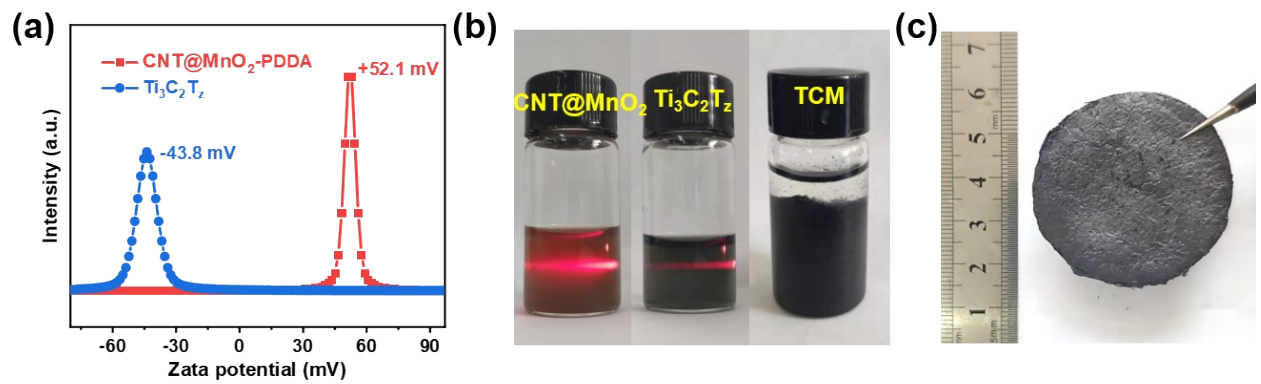


Fig. S1. (a) Zeta potentials of CNT@MnO₂-PDDA and Ti₃C₂T_x. (b) Digital images of CNT@MnO₂, Ti₃C₂T_x, and TCM suspensions. (c) Digital image of TCM freestanding film.

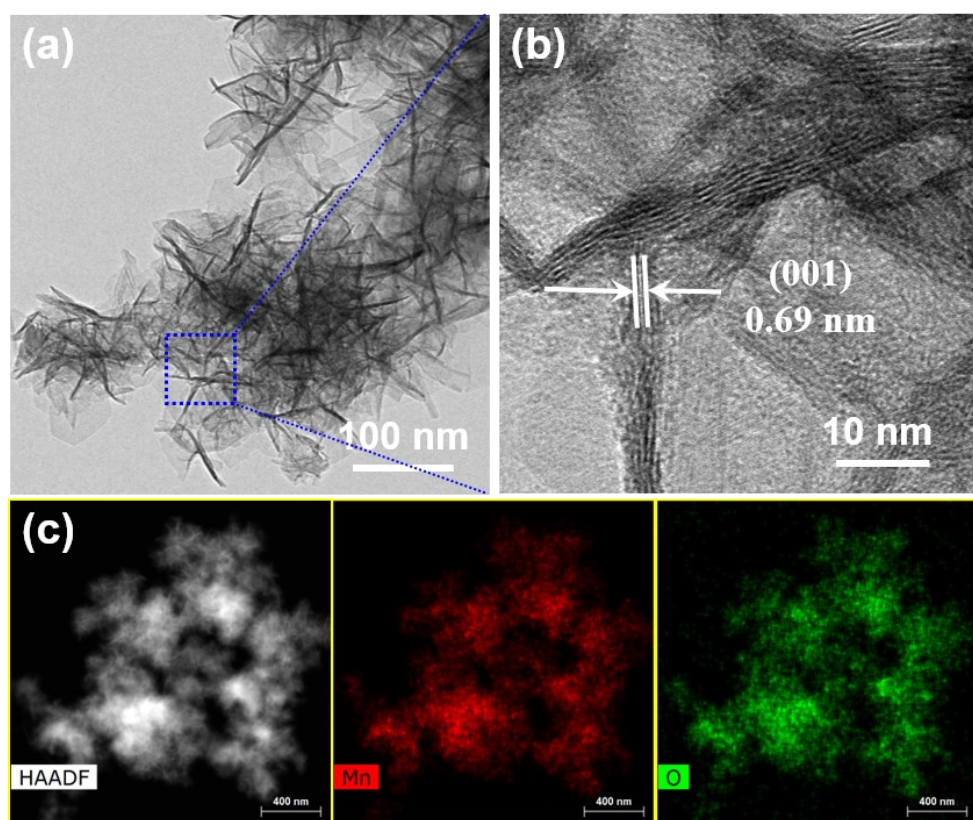


Fig. S2. (a) TEM, (b) HRTEM, and (c) EDX elemental mapping images of raw MnO_2 .

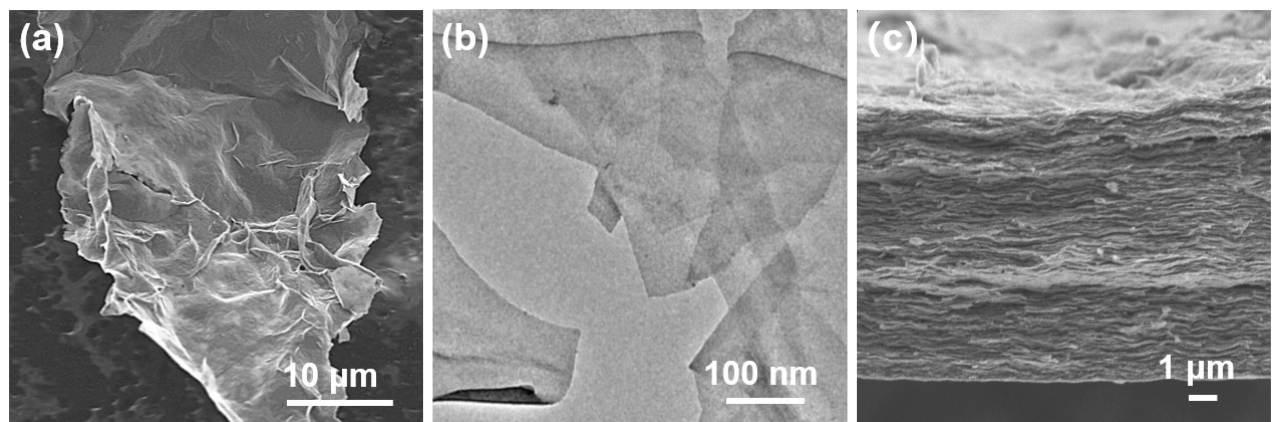


Fig. S3. (a) SEM and (b) TEM images of $\text{Ti}_3\text{C}_2\text{Tz}$. Cross-section SEM images of (c) $\text{Ti}_3\text{C}_2\text{Tz}$ membrane.

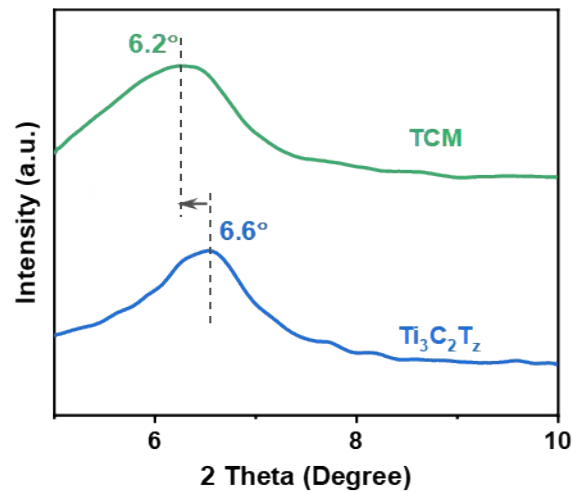


Fig. S4. XRD pattern of TCM and Ti₃C₂T_z at 5-10°.

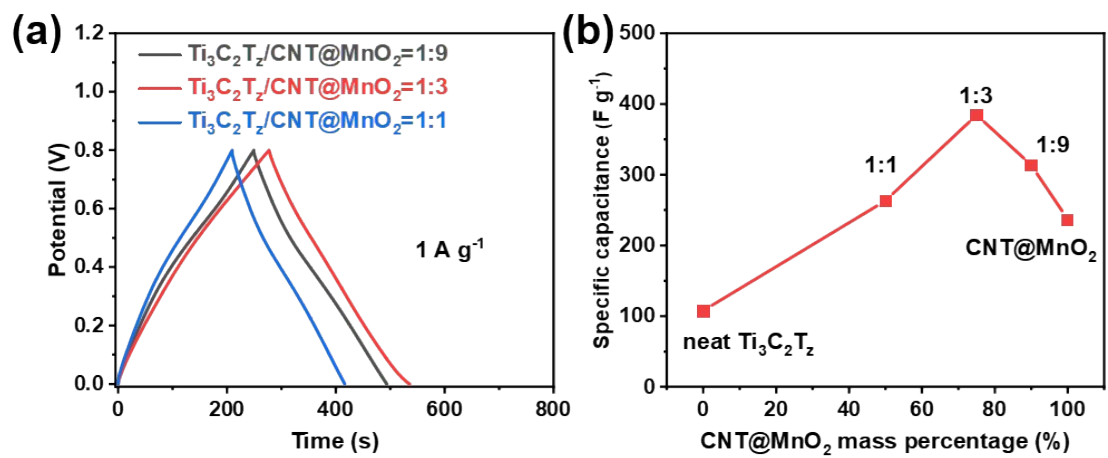


Fig. S5. (a) GCD curves and (c) Specific capacitance (0.5 A g^{-1}) comparisons for TCM:_CNT@MnO₂ = 1:9, 1:3, and 1:1.

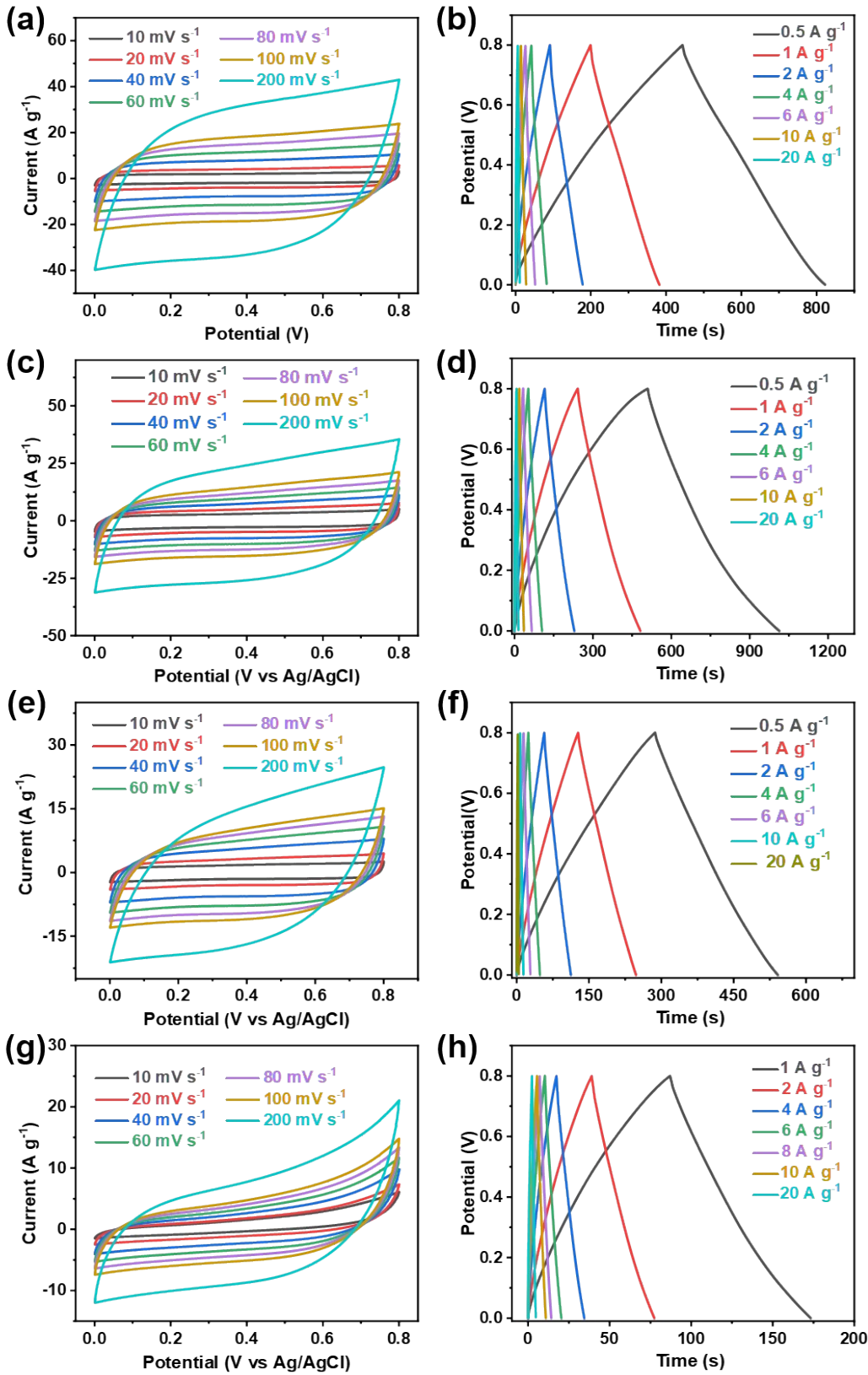


Fig. S6. (a) CV and (b) GCD curves of CNT@MnO₂ electrode. (c) CV and (d) GCD curves of MnO₂/Ti₃C₂T_x electrode. (e) CV and (f) GCD curves of MnO₂ electrode. (g) CV and (h) GCD curves of Ti₃C₂T_x electrode.

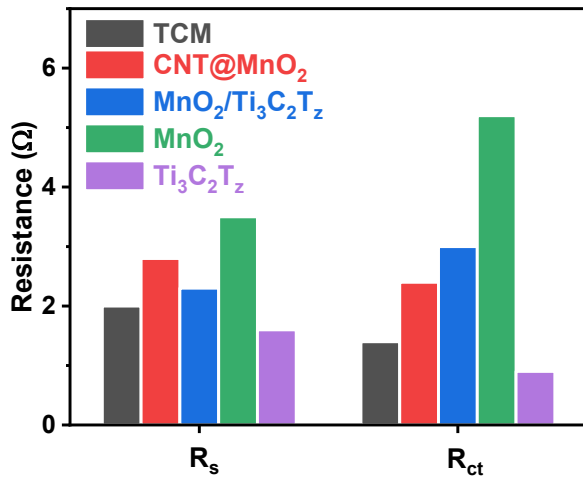


Fig. S7. Comparison of R_s , R_{ct} , and R_W for TCM, CNT@MnO₂, MnO₂/Ti₃C₂T_z, MnO₂, Ti₃C₂T_z electrodes.

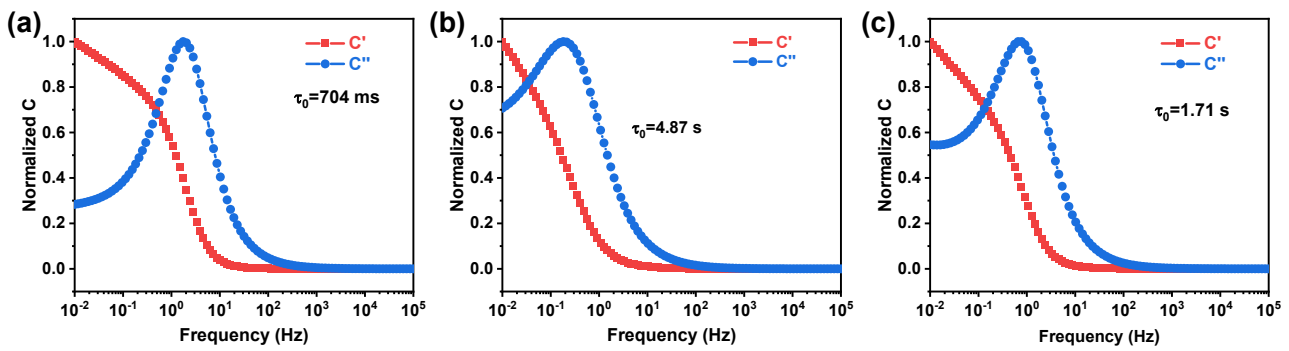


Fig. S8. Normalized real and imaginary capacitance of (a) CNT@MnO₂ electrode, (b) MnO₂ electrode, (c) Ti₃C₂T_z electrode.

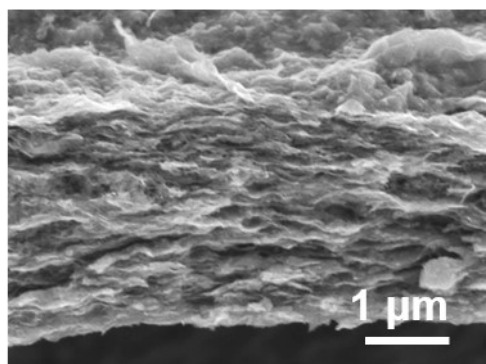


Fig. S9. SEM image of TCM film after 10000 cycles.

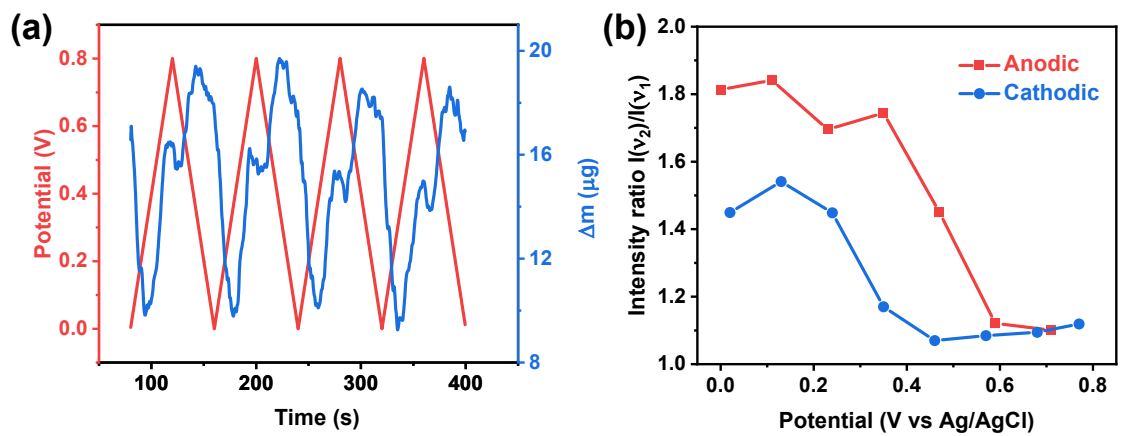


Fig. S10. (a) Electrode mass change upon potential variation during the EQCM test. (b) The relationship between the potential and the intensity ratio.

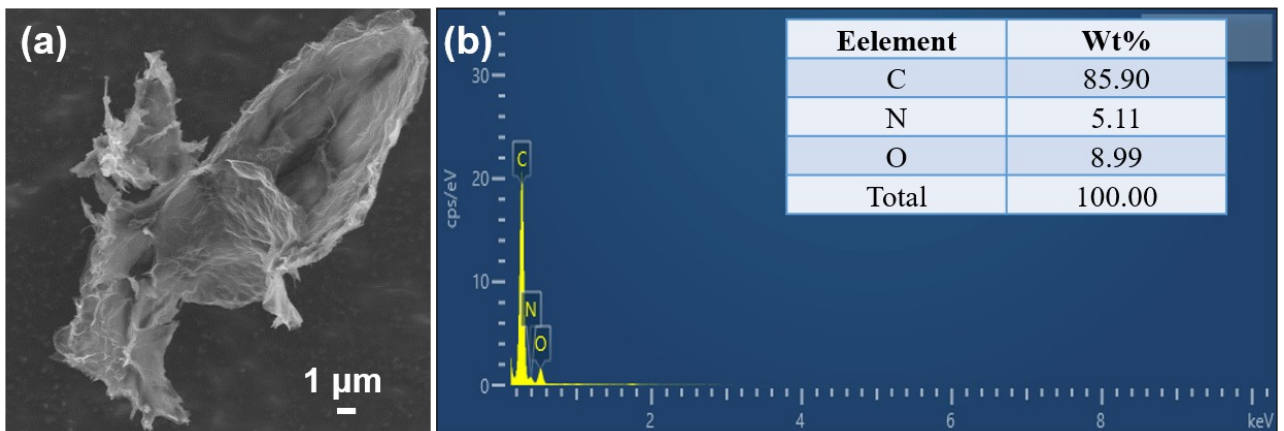


Fig. S11. (a) SEM and (c) EDX elemental mapping images of NRGO.

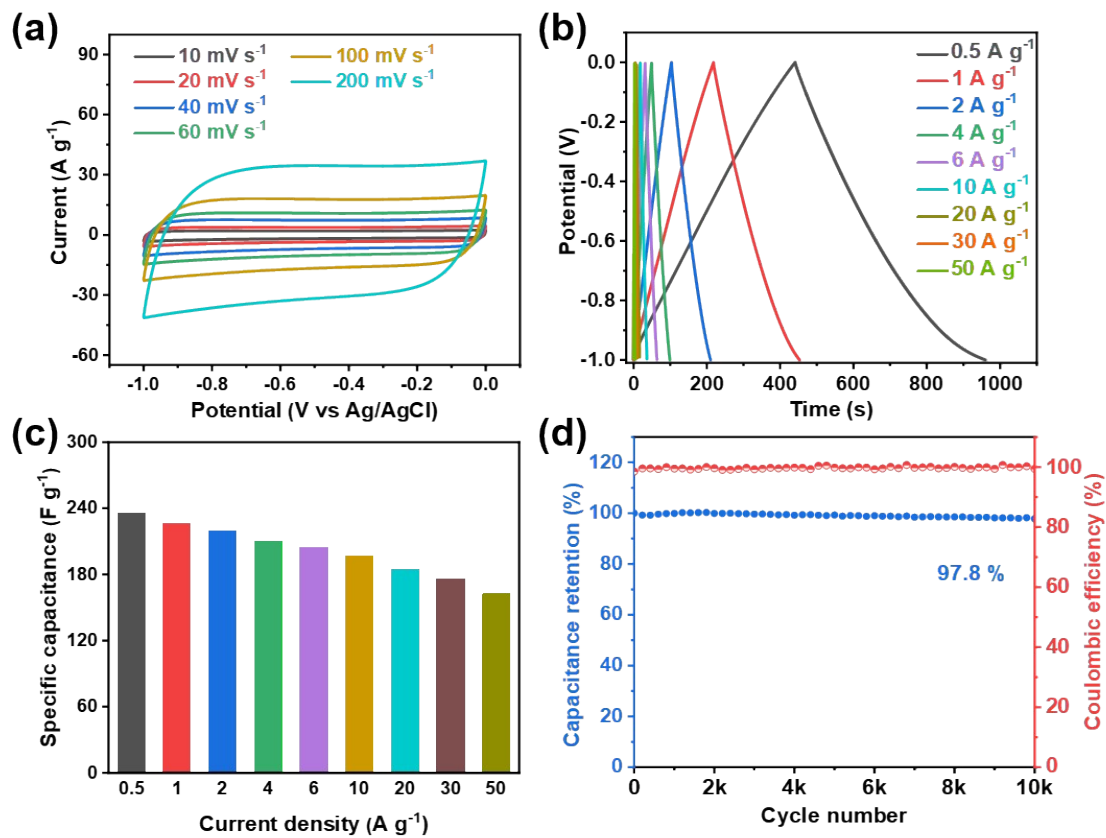


Fig. S12. (a) CV curves, (d) GCD curves, (c) rate capability, and (d) cycling stability (10 A g^{-1}) of NRGO electrode in $1 \text{ M Na}_2\text{SO}_4$.

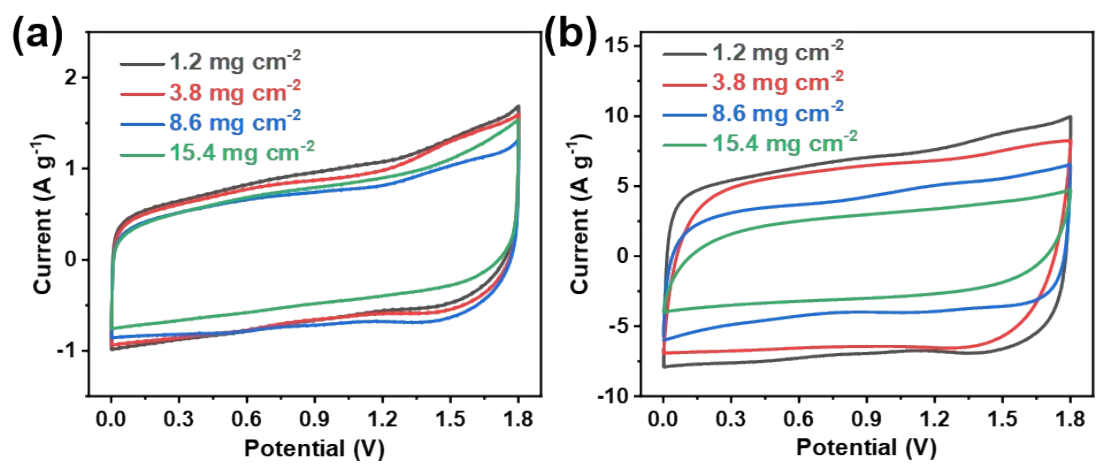


Fig. S13. CV curves at 10 mV s^{-1} and 100 mV s^{-1} for different loadings.

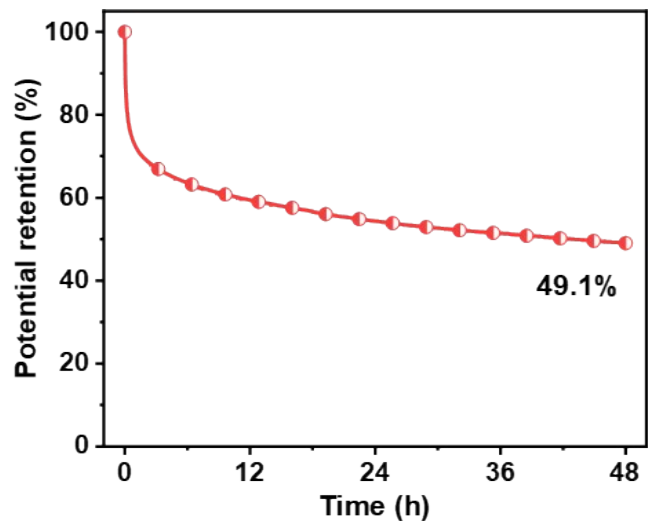


Fig. S14. Self-discharge curve of TCM//NRGO ASC.

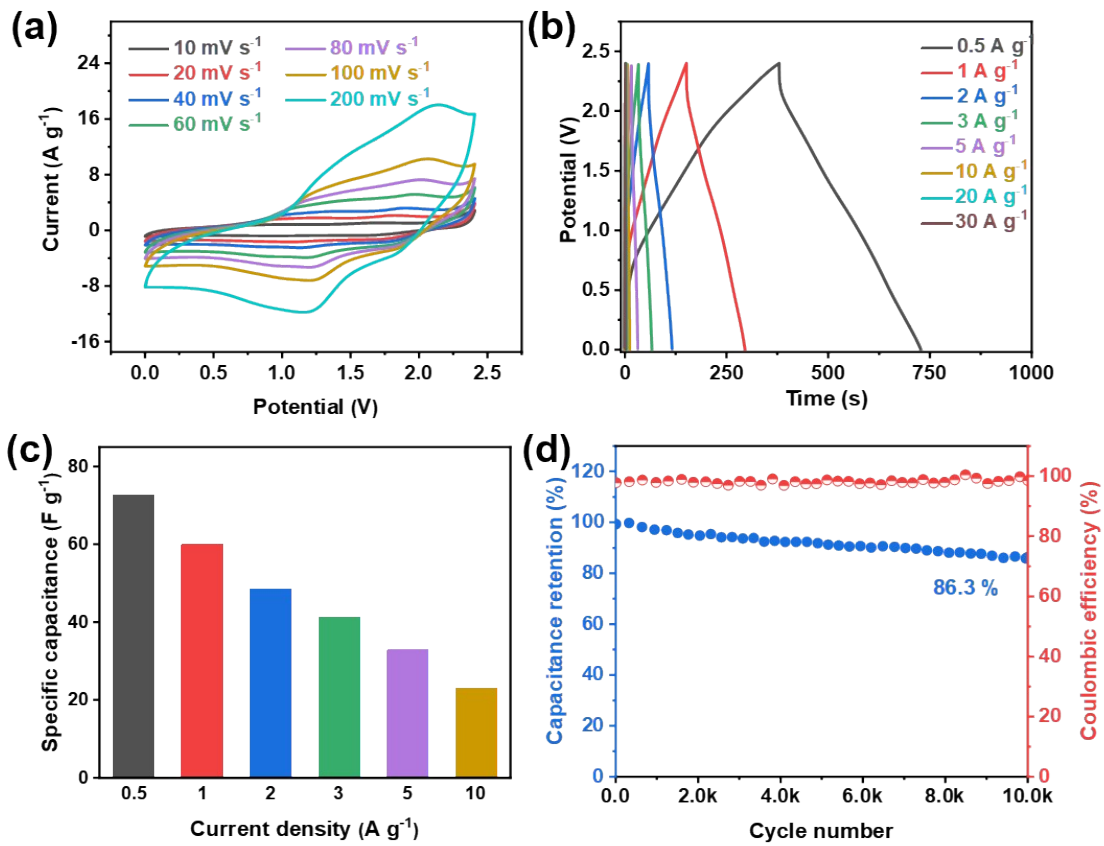


Fig. S15. (a) CV curves, (b) GCD curves, (c) rate performance, and (d) cycling stability (5 A g^{-1}) of TCM//NRGO ASC in 10 M NaClO_4 electrolyte.

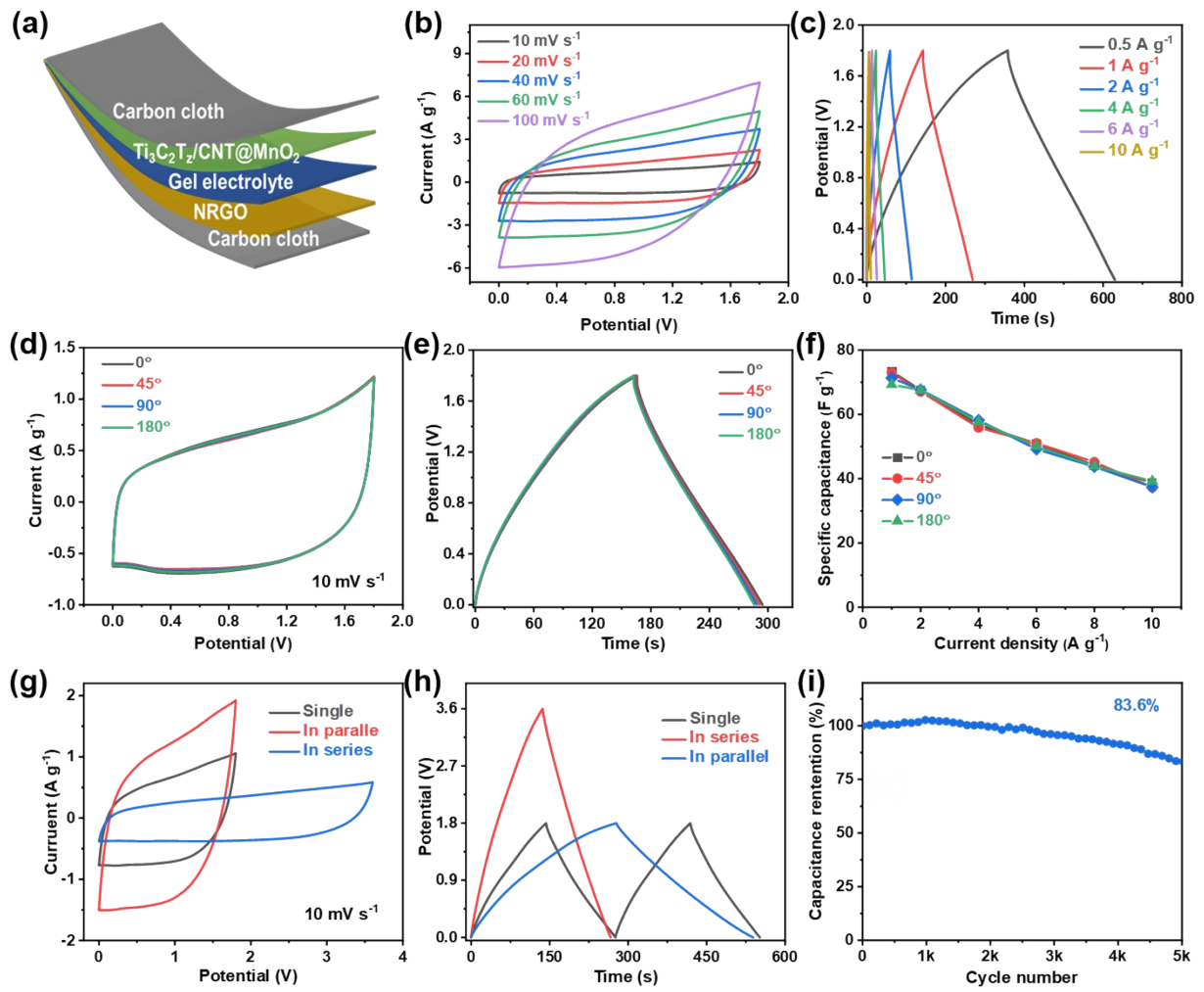


Fig. S16. (a) Schematic diagram of TCM//NRGO flexible quasi-solid state ASC with $1 \text{ M Na}_2\text{SO}_4$ gel electrolyte. (b) CV curves and (c) GCD curves of TCM//NRGO flexible quasi-solid state ASC. (d) CV curves, (e) GCD curves, and (f) rate performance of the flexible quasi-solid state ASC at different bending angle of 0° , 45° , 90° , and 180° . (g) CV and (h) GCD curves of two flexible quasi-solid-state ASCs connected in series/parallel. (i) Cycling stability (5 A g^{-1}) of TCM//NRGO quasi-solid state ASC.

Table S1. Electrochemical performance for cathode materials in comparison with those previously reported MnO₂-based electrode materials in supercapacitors.

| Electrode materials | Electrolytes | Specific capacitance | Rate capability | Cycle Performance | Ref. |
|--|---------------------------------------|--|------------------------------------|-------------------------|-----------|
| AK-MnO ₂ | 1 M Na ₂ SO ₄ | 356 F g ⁻¹ | 75% (1-50 A g ⁻¹) | 84% (5000 cycles) | 1 |
| δ-MnO ₂ | 1 M Na ₂ SO ₄ | 306 F g ⁻¹ | 38% (0.2-10 A g ⁻¹) | 83% (5000 cycles) | 2 |
| MnO ₂ /pg-C ₃ N ₄ | 1 M KOH | 348 F g ⁻¹ | 72% (1-10 A g ⁻¹) | N/A | 3 |
| MnO ₂ @PPy | 1 M Na ₂ SO ₄ | 276 F g ⁻¹ | 73% (2-20 A g ⁻¹) | 93% (1500 cycles) | 4 |
| 0.8 V-MnO ₂ | 0.5 M Na ₂ SO ₄ | 190 F g ⁻¹ | 37% (1-10 A g ⁻¹) | 91% (5000 cycles) | 5 |
| MnO ₂ @WC | 1 M Na ₂ SO ₄ | 177 F g ⁻¹ | 44% (1-30 mA cm ⁻²) | N/A | 6 |
| β-MnO ₂ /birnessite | 1 M Na ₂ SO ₄ | 306 F g ⁻¹ | 43% (5-100 mV s ⁻¹) | 92% (3000 cycles) | 7 |
| MnO ₂ @CNTs@3DGA | 1 M Na ₂ SO ₄ | 1.5 F cm ⁻¹ | 67% (1-100 A g ⁻¹) | N/A | 8 |
| MnO ₂ -C | 1 M Na ₂ SO ₄ | 287 F g ⁻¹ | 78% (1-20 A g ⁻¹) | 83.9% (10000 cycles) | 9 |
| MnO ₂ @CNT | 1 M Na ₂ SO ₄ | 337 F g ⁻¹ | 45% (1-200 mV s ⁻¹) | 92% (9000 cycles) | 10 |
| Na _{0.55} Mn ₂ O ₄ | 9.2 M NaClO ₄ | 131 F g ⁻¹ | 69% (1-16 A g ⁻¹) | N/A | 11 |
| Na _{0.25} MnO ₂ | 1 M Na ₂ SO ₄ | 295 F g ⁻¹ | 27% (2-50 A g ⁻¹) | 95.8% (10000 cycles) | 12 |
| Ti ₃ C ₂ Tz/CNT@MnO ₂ | 1 M Na ₂ SO ₄ | 384 F g ⁻¹ at 0.5 A g ⁻¹ | 61% (0.5-50 A g ⁻¹) | 92.2% (10000 cycles) | This work |

Table S2. Electrochemical performance for $\text{Ti}_3\text{C}_2\text{T}_x/\text{CNT}@\text{MnO}_2/\text{NRGO}$ ASC in comparison with previously reported devices.

| Active materials | Electrolyte | Potential (V) | E (Wh kg ⁻¹) | P (W kg ⁻¹) | Ref. |
|---|---|---------------|--------------------------|-------------------------|------------------|
| $\beta\text{-MnO}_2/\text{birnessite //AGO}$ | 1 M Na_2SO_4 | 2.2 | 40.4 | 275 | 7 |
| $\text{MnO}_2@\text{CNT}/\text{3DG //Ppy}@{\text{CNT}}/\text{3DG}$ | 1 M Na_2SO_4 | 1.8 | 18.4 | 118 | 8 |
| $\text{MnO}_2@\text{CNT //MoO}_3@\text{CNT}$ | 1 M Na_2SO_4 | 2 | 27.8 | 524 | 10 |
| $\text{Na}_{0.55}\text{Mn}_2\text{O}_4 //\text{AC}$ | 9.2 M NaClO_4 | 2.4 | 21 | 1200 | 11 |
| $\text{G}@{\text{MnO}}_2 //\text{PG}$ | 1 M Na_2SO_4 | 2 | 30.6 | 197 | 13 |
| $\text{GF/CNT/MnO}_2 //\text{GF/CNT/PPy}$ | 0.5 M Na_2SO_4 | 1.6 | 22.7 | 860 | 14 |
| $\text{Mn}_3\text{O}_4/\text{MnOOH //Ti}_3\text{C}_2\text{T}_x$ | 1 M Na_2SO_4 | 2 | 30 | 524 | 15 |
| $\text{V-MnO}_2 //\text{Mxene}$ | 1 M Li_2SO_4 | 2.1 | 46 | 283 | 16 |
| $\text{MnO}_2//(\text{Fe,Cr})_2\text{O}_3$ | 1 M Na_2SO_4 | 2 | 20.9 | 2173 | 17 |
| $\text{MnO}_2/\text{Mxene //Mxene}$ | 1 M Na_2SO_4 | 2 | 50.1 | 2100 | 18 |
| $\text{A-CNTs/K}_x\text{MnO}_2 //\text{Ti}_3\text{C}_2\text{T}_x/\text{MoO}_3$ | 1 M Na_2SO_4 | 2 | 36.4 | 863.5 | 19 |
| $\text{MnO}_2/\text{rEGO //MnO}_2/\text{rEGO}$ | 6 M KOH | 1 | 25.5 | 45 | 20 |
| $\text{MnO}_2@\text{NH}_4\text{MnF}_3 //\text{AC}$ | 1 M Na_2SO_4 | 1.7 | 40.8 | 213 | 21 |
| $\text{MnO}_2\text{-TEA //MoO}_{3-x}$ | 1 M Na_2SO_4 | 1.8 | 57.4 | 450 | 22 |
| $\text{Ti}_3\text{C}_2\text{T}_x/\text{CNT}@\text{MnO}_2 //\text{NRGO}$ | 10 M NaClO_4 | 2.4 | 58 | 596 | This work |

References

1. W. Guo, F. Yang, C. Yu, Y. Xie, J. Chen, Y. Liu, Y. Zhao, J. Yang, X. Feng, S. Li, Z. Wang, J. Yu, K. Liu, K. Qian, M. Tsige, Q. Zhang, J. Guo and J. Qiu, *Matter*, 2021, **4**, 2902-2918.
2. P. Gao, P. Metz, T. Hey, Y. Gong, D. Liu, D. D. Edwards, J. Y. Howe, R. Huang and S. T. Misture, *Nat. Commun.*, 2017, **8**, 14559.
3. Y. Shi, S. Gao, Y. Yuan, G. Liu, R. Jin, Q. Wang, H. Xu and J. Lu, *Nano Energy*, 2020, **77**, 105153.
4. W. He, C. Wang, F. Zhuge, X. Deng, X. Xu and T. Zhai, *Nano Energy*, 2017, **35**, 242-250.
5. L. Yan, C. Zhu, J. Hao, X. Liang, Y. Bai, Q. Hu, B. Tan, B. Liu, X. Zou and B. Xiang, *Adv. Funct. Mater.*, 2021, **31**, 2102693.
6. C. Chen, Y. Zhang, Y. Li, J. Dai, J. Song, Y. Yao, Y. Gong, I. Kierzewski, J. Xie and L. Hu, *Energy Environ. Sci.*, 2017, **10**, 538-545.
7. S. Zhu, L. Li, J. Liu, H. Wang, T. Wang, Y. Zhang, L. Zhang, R. S. Ruoff and F. Dong, *ACS Nano*, 2018, **12**, 1033-1042.
8. Z. Pan, M. Liu, J. Yang, Y. Qiu, W. Li, Y. Xu, X. Zhang and Y. Zhang, *Adv. Funct. Mater.*, 2017, **27**, 1701122.
9. A. Zhang, R. Gao, L. Hu, X. Zang, R. Yang, S. Wang, S. Yao, Z. Yang, H. Hao and Y.-M. Yan, *Chem. Eng. J.*, 2021, **417**, 129186.
10. T. H. Lee, D. T. Pham, R. Sahoo, J. Seok, T. H. T. Luu and Y. H. Lee, *Energy Storage Mater.*, 2018, **12**, 223-231.
11. X. Bu, Y. Zhang, L. Su, Q. Dou, Y. Xue and X. Lu, *Ionics*, 2019, **25**, 6007-6015.
12. T. Xiong, T. L. Tan, L. Lu, W. S. V. Lee and J. Xue, *Adv. Energy Mater.*, 2018, **8**, 1702630.
13. L. Wang, Y. Ouyang, X. Y. Jiao, X. F. Xia, W. Lei and Q. L. Hao, *Chem. Eng. J.*, 2018, **334**, 1-9.
14. J. Liu, L. Zhang, H. B. Wu, J. Lin, Z. Shen and X. W. Lou, *Energy Environ. Sci.*, 2014, **7**, 3709-3719.
15. W. Zheng, J. Halim, Z. Sun, J. Rosen and M. W. Barsoum, *Energy Storage Mater.*, 2021, **38**, 438-446.
16. J. Wu, Q. Li, C. E. Shuck, K. Maleski, H. N. Alshareef, J. Zhou, Y. Gogotsi and L. Huang, *Nano Res.*, 2022, **15**, 535-541.
17. P. R. Deshmukh, Y. Sohn and W. G. Shin, *Electrochim. Acta*, 2018, **285**, 381-392.

18. Z. Bo, K. Yi, H. Yang, X. Guo, Z. Huang, Z. Zheng, J. Yan, K. Cen and K. Ostrikov, *J. Power Sources*, 2021, **492**, 229639.
19. Z. Pan, C. Yang, Y. Li, X. Hu and X. Ji, *Chem. Eng. J.*, 2022, **428**, 131138.
20. H. Wang, Q. Fu and C. X. Pan, *Electrochim. Acta*, 2019, **312**, 11-21.
21. B. Li, X. Zhang, J. Dou and P. Zhang, *Electrochim. Acta*, 2020, **347**, 136257.
22. A. Zhang, R. Zhao, L. Hu, R. Yang, S. Yao, S. Wang, Z. Yang and Y.-M. Yan, *Adv. Energy Mater.*, 2021, **11**, 2101412.